Published in final edited form as:
Cell Rep. 2013 May 30; 3(5): 1389–1397. doi:10.1016/j.celrep.2013.03.040.

Chromosomal Instability Triggered by Rrm2b Loss Leads to IL-6 Secretion and Plasmacytic Neoplasms

Lufen Chang[1,*], **Robin Guo**[1], **Qin Huang**[2], and **Yun Yen**[1,3,*]

[1]Department of Molecular Pharmacology, City of Hope National Medical Center and Beckman Research Institute, Duarte, CA

[2]Division of Anatomic Pathology, City of Hope National Medical Center and Beckman Research Institute, Duarte, CA

[3]Taipei Medical University, Taipei 110, Taiwan

SUMMARY

Chronic inflammation has a tight cause-and-effect relationship with DNA damage by inflicting tissue damage and increasing cancer risk. Rrm2b, a key enzyme in *de novo* deoxyribonucleotide synthesis, is involved in DNA damage repair, but its role in cancer development has yet to be demonstrated. Rrm2b gene loss leads to severe numerical and structural chromosome abnormalities that cause ATM activation, inducing p-Ser85 IKKγ/NEMO and IκB kinase (IKK). NF-kB consequently induced by IKK triggered sustained IL-6 expression that constitutively activates STAT3 in Rrm2b-deficient cells. High plasma IL-6 and associated hematologic disorders were observed in *Rrm2b*$^{-/-}$ mice. 30–40% of aged Rrm2b heterozygous knockout mice developed plasma cell neoplasms and suffered from progressive splenomegaly and ascites. The genetic ablation of IL-6 suppressed STAT3 induction and delayed disease onset in *Rrm2b*$^{-/-}$ mice, extending their life span. Thus, Rrm2b serves a crucial role in maintaining chromosomal stability and preventing chronic inflammation-associated tumorigenesis.

Keywords

Chronic inflammation; IL-6; DNA damage; Plasmacytic neoplasms; and Rrm2b

INTRODUCTION

Chronic inflammatory responses disrupt tissue homeostasis and promote cancer development and progression (Grivennikov et al., 2010). It was postulated that activated inflammatory cells serve as a source of reactive oxygen species (ROS) capable of inducing DNA damage and genomic instability. Conversely, DNA damage might also lead to

*Corresponding authors: Lufen Chang, Ph.D., Assistant Research Professor, Department of Molecular Pharmacology, 626-256-4673 ext. 64376, lchang@coh.org. Yun Yen, M.D., Ph.D., Professor and Chair, Department of Molecular Pharmacology and Associate Cancer Center Director for Translational Research, 626-256-4673 ext. 65707, yyen@coh.org FAX: 256-471-3607.

SUPPLEMENTARY INFORMATION

The supplemental information includes **Extended Experimental Procedures** and **four Figures** that can be found with this article online.

inflammation and promote tumorigenesis (Rodier et al., 2009). Current cancer treatment by radiation therapy or DNA damaging chemotherapeutic drugs may result in inflammation that can stimulate tumor growth. Uncovering the molecules that trigger chronic inflammation associated with sustained DDR signaling could lead to a deeper understanding of cancer development and effective strategies in cancer prevention.

DNA damage triggers the DDR in cells through a signal amplification cascade (Rodier et al., 2009). The DDR in reversible DNA damage transiently arrests proliferating cells as DNA is repaired. However, cells with irreparable DNA damage, often caused by strong genotoxic stresses, present with persistent DNA damage foci (PDDF), which are detectable by the presence of 53BP1 and H2AX (Rodier et al., 2009). These cells express a wide range of chemokines and cytokines (such as IL-6, IL-8, MMP3, and CXCL1), known as the senescence-associated secretary phenotype (SASP), are mediated by ATM but not by senescence regulators. IL-6 and IL-8 corresponding to ATM expression were found in premalignant breast lesions (Rodier et al., 2009). There is increasing evidence demonstrating that DNA damage can lead to inflammation and thereby promote tumorigenesis. The murine model of hepatocellular carcinoma was induced by the carcinogen diethylnitrosamine (DEN), in which DNA damage contributes to necrotic cell death, resulting in an inflammatory reaction that promotes tumor development (Maeda et al., 2005). Defective DNA repair caused by a deficiency of the Fen1 exonuclease also results in a tumor promoting inflammatory response that is driven by damaged DNA (Zheng et al., 2007).

Ribonucleotide reductase (RR) plays an essential role in supplying deoxyribonucleoside triphosphate (dNTPs) for DNA synthesis and repair. The RR holoenzyme consists of a heterodimeric tetramer of nonidentical homodimers of large Rrm1 (R1) and small Rrm2 (R2) or Rrm2b (p53R2) subunits (Nordlund and Reichard, 2006). dNTP is provided by the R1–R2 complex in S phase. In the G0/G1 phase following DNA-damage stress, dNTPs for nuclear DNA synthesis and repair are supplied by Rrm2b (Tanaka et al., 2000). The R1-Rrm2b complex also contributes dNTPs for basal DNA repair and mitochondrial DNA synthesis in quiescent cells without external DNA damage stress (Bourdon et al., 2007). Despite evidence supporting Rrm2b's involvement in DNA damage repair, its role in cancer development *in vivo* is not yet defined.

Rrm2b can also be regulated at the post-translational level by ATM during the acute phase of the genotoxic stress response and is associated with the MRE11 complex (Chang et al., 2008). Our earlier findings linking Rrm2b to ATM strongly suggest a potential role of Rrm2b in DDR and disease development. In this study, we investigated this possibility using Rrm2b knockout mice. Rrm2b homozygous knockout ($Rrm2b^{-/-}$) mice did not live long enough for cancer to be observed. In contrast, Rrm2b heterozygous knockout ($Rrm2b^{+/-}$) mice are developmentally normal and fertile. Some $Rrm2b^{+/-}$ mice developed chronic inflammation and plasma cell neoplasia after nine months of age and showed signs of morbidity. This study is the first to show that Rrm2b-deficient mice provide an important murine model for understanding chronic inflammatory states as well as neoplastic diseases in the context of persistent DDR signaling and chronic inflammatory cytokine secretion.

RESULTS

Constitutive NF-KB and STAT3 Mediate Sustained IL-6 Expression in Rrm2b-Deficient Cells

To address whether RRM2b participates in ATM signaling in response to genotoxic stress, we first compared the activities of ATM and its downstream substrates between $Rrm2b^{+/+}$ and $Rrm2b^{-/-}$ primary MEFs by immunoblot (IB) analysis. Activated ATM and γH2AX were more apparent in $Rrm2b^{-/-}$ than $Rrm2b^{+/+}$ wild-type (WT) MEFs (Figure 1A).

Additionally, a number of ATM/ATR substrates were more highly activated in *Rrm2b*$^{-/-}$ MEFs than in *Rrm2b*$^{+/+}$ MEFs, as determined by an antibody directed against phosphorylated Ser or Thr residues in the ATM/ATR substrate motif. ATM and NBS1 protein levels were similar between *Rrm2b*$^{+/+}$ and *Rrm2b*$^{-/-}$ MEFs (Figure 1A). Deletion of Rrm2b also did not change the protein levels of other RR subunits, RRM1 and RRM2 (Figure S1A). The ATM signaling cascade can regulate a range of chemokines and cytokines (Rodier et al., 2009). Thus we used multiplex cytokine analysis to further analyze the cytokine/chemokine profile in culture medium from *Rrm2b*$^{+/+}$ and *Rrm2b*$^{-/-}$ MEFs at passage-2 before and after IR exposure. No significant difference in cytokine/chemokine levels were observed between the two cell types except for interleukin-6 (IL-6) and monocyte chemoattractant protein-1 (MCP-1) (Figures 1B). Compared to *Rrm2b*$^{+/+}$ MEFs, IL-6 and MCP-1 proteins were already 3-fold higher in *Rrm2b*$^{-/-}$ MEF media prior to IR exposure (Figure 1B). IL-6 and MCP-1 productions in WT cells can be induced by a high (10 Gy) but not by a low (1 Gy) dose of IR (Figure 1B). However, production of endogenous IL-6 and MCP-1 by *Rrm2b*$^{-/-}$ MEFs was not further induced by 10 Gy IR, indicating that *Rrm2b*$^{-/-}$ MEFs already constitutively secreted both cytokines at maximal levels. Constitutive IL-6 and MCP-1 secretion also corresponded to high endogenous amounts of *IL-6* and *MCP-1* RNA transcripts in *Rrm2b*$^{-/-}$ MEFs (Figure 1C). *IL-6* and *MCP-1* genes can be regulated by NF-κB, which has been shown to be a predominant transcription factor in mediating downstream target genes of ATM (Wu et al., 2006). We next evaluated if constitutive ATM activity in *Rrm2b*$^{-/-}$ MEFs also altered NF-κB activity. NF-κB activity is modulated by the inhibitor IKBα, which is in turn negatively regulated by the IKK complex comprised of two catalytic subunits, IKKα and IKKβ, and the scaffolding protein IKKγ/NEMO (Grivennikov et al., 2010). The levels of IKKα and IKKβ as well as total NF-κB proteins were similar between *Rrm2b*$^{+/+}$ and *Rrm2b*$^{-/-}$ MEFs, whereas IKKγ proteins were slightly elevated in *Rrm2b*$^{-/-}$ MEFs (Figure 1D). The IKKγ/NEMO proteins were also highly phosphorylated at serine 85, which is known to be dependent on ATM in response to genotoxic stress (Wu et al., 2006). Phosphorylated IKKγ/NEMO in *Rrm2b*$^{-/-}$ MEFs caused a 2-fold higher IKK kinase activity when compared to *Rrm2b*$^{+/+}$ MEFs (Figure 1E). Consequently, IKBα, a repressor of NF-κB activity, accumulated much less in *Rrm2b*$^{-/-}$ MEFs compared to WT (Figure 1D). Constitutive DNA binding activity of both NF-κB and STAT3 were 2–3 fold higher in *Rrm2b*$^{-/-}$ MEFs than *Rrm2b*$^{+/+}$ MEFs (Figure 1F). mRNAs of a number of *IL-6* downstream target genes, such as *STAT3*, *c-MYC*, and *JAGGED1* were correspondingly elevated in *Rrm2b*$^{-/-}$ MEFs before and after exposure to IR (Figures S1B). STAT3 protein levels also accumulated more in *Rrm2b*$^{-/-}$ MEFs than *Rrm2b*$^{+/+}$ MEFs (Figure 1D). Reconstitution of *Rrm2b*$^{-/-}$ fibroblasts with a lentivirus encoding *Rrm2b* gene was able to suppress the expression of *IL-6*, but not *MCP-1* (Figure 1G). These data suggest that induction of *IL-6* may represent a direct consequence of *Rrm2b* deficiency or a positive regulatory response to *Rrm2b* deficiency. ATM knockdown reduced *IL-6* induction by more than 50% (Figure 1H). 50 to 70% depleted STAT3 was able to reduce *IL-6* induction by 20 to 30% significantly. A significant 30% reduction of *IL-6* can also be achieved by inactivation of NF-κB activity in *Rrm2b*$^{-/-}$ MEFs with forced expression of adenoviral IkBα super-repressors (IkBα S32A/S36A) (Figure 1H). We also investigated if constitutive IL-6 induction triggered by Rrm2b deficiency can be attributed to senescence. There were actually less senescent *Rrm2b*$^{-/-}$ MEFs compared to *Rrm2b*$^{+/+}$ MEFs at both low (passage-2) and high (passage-11) passages (Figure S1C). IL-6 and MCP-1 transcription levels were even higher in *Rrm2b*$^{-/-}$ than in *Rrm2b*$^{+/+}$ MEFs at passage-2, whereas p16 and p53 mRNAs were similar between both cell types (Figure S1D). At passage-11, both *IL-6* and *MCP-1* RNAs were significantly elevated in *Rrm2b*$^{-/-}$ MEFs than *Rrm2b*$^{+/+}$ MEFs (Figure S1D). *IL-6* and *MCP-1* RNAs were not yet induced in high-passage *Rrm2b*$^{+/+}$ MEFs despite increased senescence. *Rrm2b*$^{-/-}$ MEFs also showed increased cyclin D1 proteins (Figure S1F) and demonstrated rapid cellular growth (Figure S1E). Knockdown of senescence regulator p16 (Figure S1G) or p53 (Figure S1H) resulted in

slightly increased IL-6 in *Rrm2b*$^{-/-}$ MEFs. Taken together, in the context of Rrm2b deficiency, IL-6 induction through NF-κB and STAT3 depended on ATM but not senescence regulators (p16 and p53).

Loss of *Rrm2b* Gene Causes Chromosomal Instability

To directly identify chromosomal abnormality of any forms or frequencies, we analyzed MEFs by spectral karyotype (SKY) analysis (Figure 2). SKY was performed on MEFs at passage one to minimize the effects of extended cell culture passaging. The data indicated that nearly all the examined chromosomes from *Rrm2b*$^{+/+}$ MEFs had only one break (Figures 2A and 2B). In addition to chromatid breakages, severe forms of chromosomal abnormalities, including deletion, loss, and translocation were identified in *Rrm2b* haploinsufficient (*Rrm2b*$^{+/-}$) MEFs. Deletion of both *Rrm2b* alleles created additional chromosomal abnormalities, including gains, duplications, and isochromosomes (Figures 2A and 2B). The total spontaneous aberrations from each chromosome in *Rrm2b*$^{-/-}$ MEFs were almost 100-fold and 5-fold higher compared with *Rrm2b*$^{+/+}$ and *Rrm2b*$^{+/-}$ MEFs, respectively (Figure 2A). After exposure to 1 Gy IR, additional forms of chromosomal abnormalities (derivative and dicentric chromosomes) were observed in *Rrm2b*$^{-/-}$ MEFs, whereas chromatid breakages were the only type of abnormality found in *Rrm2b*$^{+/+}$ MEFs (Figure 2C). Excluding chromatid breakages, there was almost a 300-fold increase in IR-induced chromosomal aberration frequencies in *Rrm2b*$^{-/-}$ MEFs compared to *Rrm2b*$^{+/+}$ MEFs (Figure 2A). These results demonstrate that Rrm2b is involved in preserving the integrity of chromosomal number and structure, thereby helping to maintain genetic stability. The same batch of MEFs which were analyzed for genetic abnormality in Figure 2 were also analyzed for DDR signaling and IL-6 expression at a single cell level by immunocytochemistry (ICC) (Figure S2). Compared to *Rrm2b*$^{+/+}$ MEFs, *Rrm2b*$^{-/-}$ MEFs showed robust IL-6, p-ATM, and γH2AX signals (compare Figures S2A to S2B, S2D to S2E and S2G to S2H). Distinct nuclear p53 binding protein-1 (53BP1) foci formation accumulated robustly in *Rrm2b*$^{-/-}$ MEFs (compare Figure S2J to S2K). IL-6, p-ATM, γH2AX and 53BP-1 signals in *Rrm2b*$^{+/+}$ MEFs were low prior to IR but higher following exposure to 4 Gy IR (Figures S2C, S2F, S2I and S 2L). Nuclear Rrm2b expression in *Rrm2b*$^{+/+}$ MEFs (Figure S2M) appeared to be specific as it was completely absent in *Rrm2b*$^{-/-}$ MEFs (Figure 2N).

Mice Deficient in Rrm2b Exhibit Elevated IL-6 and Hematologic Disorders

Next, we assessed whether losing the *Rrm2b* gene can cause a change of IL-6 and MCP-1 expression in mice tissue. Loss of the *Rrm2b* gene resulted in a dose-dependent effect on *IL-6* gene induction in bone marrows (Figure 3A). *IL-6* RNA levels in *Rrm2b*$^{-/-}$ bone marrows were four-fold higher than that of *Rrm2b*$^{+/+}$ bone marrows, whereas *IL-6* levels in *Rrm2b*$^{+/-}$ bone marrows were intermediate to those of the two genotypes (Figure 3A). Similar outcomes were observed in 1-month-old mice blood where the loss of one or both *Rrm2b* genes corresponded to increases in serum IL-6 and MCP-1 protein levels in a dose-dependent manner (Figure 3B). Accumulation of MCP-1 and, especially, IL-6 continued in 9- to 12-month-old *Rrm2b*$^{+/-}$ mice but not in age-matched *Rrm2b*$^{+/+}$ littermates (Figure 3C). Unfortunately, *Rrm2b*$^{-/-}$ mice did not survive longer than seven weeks after birth. Beginning at seven months, some *Rrm2b*$^{+/-}$ mice developed severely hemorrhagic splenomegalies (Figure 3D). Therefore, we monitored various organ weights and the total body weight from the 7- to 9-month-old *Rrm2b*$^{+/+}$ and *Rrm2b*$^{+/-}$ mice and found that found that spleens from Rrm2b$^{+/-}$ mice were substantially and significantly larger than those from Rrm2b$^{+/+}$ mice, whereas other organs were comparable in size and weight (Figure S3A). The liver was slightly enlarged in *Rrm2b*$^{+/-}$ mice as compared with the normal counterparts, but the difference between two genotypes was insignificant (Figure S3A). Histologic examination of *Rrm2b*$^{+/-}$ spleen sections at different ages also showed signs of progressive

pathology. The white pulps of *Rrm2b*$^{+/-}$ and *Rrm2b*$^{-/-}$ spleens were larger and more in number than those of *Rrm2b*$^{+/+}$ spleens at 1-month of age (Figure 3E). At 12 months, the architecture of *Rrm2b*$^{+/-}$ spleen appeared remarkably disorganized as marginal zones disappeared and the red and white pulps became indistinguishable (Figures 3F). Clusters of CD138+ (a plasma cell marker) plasmacytoid infiltrate were also observed in *Rrm2b*$^{+/-}$ spleens (Figure 3G). These compactly arranged plasmocytoid cells appeared to be monoclonal, which selectively expressed the immunoglobulin (Ig) KAPPA, but not LAMBDA, light chain (Figure 3G). Furthermore, plasma cell numbers were more than 5-fold higher in *Rrm2b*$^{+/-}$ than in *Rrm2b*$^{+/+}$ bone marrows (Figure 3H). In contrast, less than 1% of *Rrm2b*$^{+/-}$ expressed B220, a marker of early pro-B cells, whereas approximately 15% of the *Rrm2b*$^{+/+}$ bone marrow population were B220 positive (Figure 3H). These results indicated that most of the populations of B cells in aged *Rrm2b*$^{+/-}$ mice were plasma cells. An elevated plasma cell count should lead to an abnormal amount of antibody production. As expected, abnormal Ig levels were found in mice deficient in the *Rrm2b* gene (Figure S3). IgA and IgE levels were similar in young and old mice regardless of genotype (Figures S3B and S3C). However, in younger mice, IgM levels increased and IgG levels decreased significantly with the loss of *Rrm2b* gene in a dose-dependent manner (Figures S3D and S3E). Serum IgG levels were nearly undetectable in *Rrm2b*$^{-/-}$ mice (Figure S3E). With age, *Rrm2b*$^{+/-}$ mice developed significantly higher serum IgM levels than age-matched *Rrm2b*$^{+/+}$ mice (Figure S3D). Conversely, IgG levels were significantly lower in aged *Rrm2b*$^{+/-}$ mice compared to *Rrm2b*$^{+/+}$ mice (Figure S3E). Defective B cell development and abnormal serum Ig levels in Rrm2b-deficient mice prompted us to analyze the complete blood count (CBC) profiles of these mice. Significantly higher levels of WBC, lymphocyte, and neutrophil were found in 1-month-old *Rrm2b*$^{-/-}$ mice compared to *Rrm2b*$^{+/+}$ littermates (Figure S3F). *Rrm2b*$^{+/-}$ mice had cell counts intermediate to that of *Rrm2b*$^{-/-}$ and *Rrm2b*$^{+/+}$ littermates, indicating an *Rrm2b* gene dose-dependent effect in the development of blood cell lineages. Aged and sick *Rrm2b*$^{+/-}$ mice developed even more significantly elevated levels of WBC and lymphocyte counts than their WT littermates (Figure 3I). Some *Rrm2b*$^{+/-}$ mice also presented with hair loss, skin infections, and enlarged lymphoid nodes (Figures S3H, S3J and S3L). Some of sick *Rrm2b*$^{+/-}$ mice even had a ruptured spleen and liver and developed ascites close to 12 months (Figure S3M). Abnormally high monoclonal plasma cells, Ig levels and WBC counts are hallmarks of patients suffering from plasma cell neoplasms, including multiple myeloma and plasmacytoma (Naugler and Karin, 2008).

The Effect of Crossing *Rrm2b*$^{-/-}$ Mice with IL-6-deleted Mice

The observation that IL-6 production was increased in Rrm2b-deficient cells and mice led us to investigate the contribution of this cytokine to disease in *Rrm2b*$^{-/-}$ mice. *Rrm2b*$^{+/-}$ and *IL-6*$^{+/-}$ heterozygote mice were crossed to generate *Rrm2b*$^{-/-}$*IL-6*$^{-/-}$ double mutants. Hemorrhaging was not apparent in 1-month-old *Rrm2b*$^{-/-}$*IL-6*$^{-/-}$ and 11-month-old *Rrm2b*$^{+/-}$*IL-6*$^{-/-}$ spleens (Figure 4A). Abnormal IgM (Figure 4SA) and IgG (Figure 4SB) levels in *Rrm2b*$^{+/-}$ and *Rrm2b*$^{-/-}$ mice were restored to a range similar to *Rrm2b*$^{+/+}$ littermates after IL-6 deletion. The CBC profiles from *Rrm2b*$^{-/-}$*IL-6*$^{-/-}$ and *Rrm2b*$^{+/-}$*IL-6*$^{-/-}$ mice were also similar to their WT littermates (Figures S4C and S4D). Elevated STAT3 (89 kDa) proteins and phoshorylation (Ser727) levels (Figure 4B) as well as mRNAs of *IL-6* downstream genes (*STAT3*, *c-Myc*, *Notch,* and *Jagged 1*) (Figure 4C) in old *Rrm2b*$^{+/-}$*IL-6*$^{-/-}$ bone marrows were suppressed following *IL-6* deletion. The removal of IL-6 dramatically reduced urine protein secretion and glomerulopathy (Figures 4D and S4E). Despite extensive genomic abnormalities in *Rrm2b*$^{-/-}$ MEFs, elimination of the *IL-6* gene was still able to extend the life of *Rrm2b*$^{-/-}$ mice by 8 to 10 weeks (Figure 4E). The mortality of *Rrm2b*$^{+/-}$*IL-6*$^{-/-}$ mice was undetectable at 9 to 14 months compared to 30–40% in *Rrm2b*$^{+/-}$*IL-6*$^{+/+}$ mice of the same age (Figure 4E). Most importantly, bone marrow myeloma cells of multiple myeloma patients (N=41) showed a significantly 3-fold decrease

in Rrm2b and 5-fold increase in IL-6 expression compared to those of normal human bone marrows. Rrm2b levels inversely correlated with IL-6 expression in MM patients (the ρ values of Pearson's correlation coefficient = − 0.9014).

DISCUSSION

DNA damage caused by depleted dNTP pools can trigger ATM-Chk2-like S-phase checkpoint pathway (Kumar et al., 2011). Elevated ATM activity induced by attenuated dNTP pools in Rrm2b-deficient MEFs might serve as a genome surveillance mechanism. In addition to orchestrating cell-cycle checkpoints, ATM stimulates the secretion of proinflammatory cytokines induced by irreparable DNA damage (Rodier et al., 2009). Chromosomal abnormalities in Rrm2b-deficient MEFs (Figure 2) could have led to irreparable DNA damage and constitutive DDR signaling, resulting in the autonomous secretion of cytokines, including IL-6 and MCP-1 (Figure 1). Our data confirms previous findings that persistent DDR-induced *IL-6* mRNA in $Rrm2b^{-/-}$ MEFs can be suppressed greater than 50% by shRNA against *ATM* (Figure 1). Rrm2b was previously shown to be associated with the ATM and the MRN complex (Chang et al., 2008). In addition to supplying dNTPs, Rrm2b might interact with the ATM and the MRN complex to maintain chromatin stability. Therefore, constitutive ATM activation by Rrm2b deficiency may be potentially attributed to a mechanism independent of dNTP depletion.

NF-κB and STAT3 are central signalling hubs in regulating inflammation-mediated tumour promotion and metastasis (Grivennikov et al., 2010). Cooperative signaling through the NF-κB and STAT3 pathways has been found in numerous cancers. Although through distinct mechanisms, activated NF-κB and STAT3 can either synergistically or individually control the expression of anti-apoptotic, pro-proliferative, and proinflammatory cytokine genes to promote tumorigenesis. IL-6 has been implicated as a potential mediator between NF-κB and STAT3 (Grivennikov and Karin, 2008). Here we demonstrate that aberrant activation of NF-κB induced by ATM-IKK led to the stimulation of STAT3 and consequent IL-6 release, providing novel evidence of a cross-talk between NF-κB and STAT3 signaling in the context of genome instability triggered by Rrm2b deficiency. The interplay between NF-κB and STAT3 might make it difficult to completely blunt IL-6 induction by the mere disruption of either NF-κB or STAT3 signaling (Figure 1H).

IL-6, a multifunctional pro-inflammatory cytokine, is involved in cell survival, apoptosis, proliferation, immune responses, and tumorigenesis (Naugler and Karin, 2008). The role of IL-6 in carcinogenesis is especially pronounced in multiple myeloma (MM), a neoplasm of plasma cells. Renal failure is a major cause of mortality in multiple myeloma patients. Similar to previous observations (Kimura et al., 2003; Powell et al., 2005), we also observed that severe kidney failure with marked proteinuria is a primary cause of death (FigureS4E). Additional to onset of kidney failure, we demonstrated that $Rrm2b^{-/-}$ mice developed dysfunctional immunologic and hematopoietic systems (high serum IL-6, splenic hemorrhage, abnormal IgM and IgG levels, lymphocytosis, neutrophilia, and thrombocytosis). Furthermore, some aged $Rrm2b^{+/-}$ mice developed a plasmacytoma-like neoplasm, progressive splenomegaly, enlarged lymph nodes and ascites. Blockade or modulation of the IL-6 signal is a strategy that is well on its way to clinical trials for lymphoma, multiple myeloma (MM) and chronic inflammatory diseases (Naugler and Karin, 2008). Interestingly, $Rrm2b^{-/-}IL\text{-}6^{-/-}$ mice lived longer than $Rrm2b^{-/-}$ mice by two more months (Figure 4E). Splenic hemorrhage, abnormal hematologic parameters and proteinuria were dramatically reduced in $Rrm2b^{-/-}IL\text{-}6^{-/-}$ double mutants (Figure 4). Similar to their age-matched WT littermates, kidney and spleen samples from $Rrm2b^{-/-}IL\text{-}6^{-/-}$ showed no pathologic findings. These results strongly suggest that IL-6

partly contributes to the development of hematologic disorders and mortality from renal failure in *Rrm2b*$^{-/-}$ mice.

Our findings demonstrate a potential role of Rrm2b in prohibiting oncogenesis. Earlier data implicated that Rrm2b protein level might be negatively correlated to cancer progression (Liu et al., 2011; Zhang et al., 2011). Based on the observed phenotypes from Rrm2b-deficient mice model, Rrm2b deficiency might be a potential risk factor for hematologic malignancy. Indeed, Rrm2b proteins were much reduced in myeloma cells of MM patients (Figure 4F). *Rrm2b* deletion, mutation or haploinsufficiency can serve as a diagnostic marker in MM or other lymphomas. Finally, Rrm2b reduction could potentially be used in personalized medicine to identify patients who are susceptible to the inflammatory side effects and cancer risk of traditional radiation therapy or DNA-damaging chemotherapeutic drugs.

EXPERIMENTAL PROCEDURES

Mice and Cell Culture

Generation of *Rrm2b*$^{-/-}$ mice by the gene trap method has been described (Powell et al., 2005). *Rrm2b*$^{+/-}$ mice in mixed genetic background (129/SvEvBrd and C57BL/6J) were obtained from the Texas A&M Institute for Genomic Medicine (TIGM) and backcrossed to C57BL/6J mice for 7 generations. *IL-6*$^{-/-}$ mice (stock number: 002650, C57BL/6J background) were purchased from The Jackson Laboratory. MM specimens (IRB10046) were obtained from the tissue bank of Translational Research Core (TLR) at City of Hope. Murine studies were carried out in accordance with protocols approved by the Institutional Animal Care and Use Committee (IACUC) of City of Hope. *In vitro* MEFs experiments using the mice that have been had been backcrossed to C57BL/6 for at least 7 generations, except for *Rrm2b*$^{-/-}$ fibroblasts (Figure 1F) which were derived from mouse embryos in mixed sv129 and C57BL/6 background (Tanaka et al., 2000).

Supplementary Material

Refer to Web version on PubMed Central for supplementary material.

Acknowledgments

We gratefully thank Michael Karin (UCSD) for his review and comments on our manuscript, Yibin Wang (UCLA) for adenoviruses expressing IκBα mutant super-repressor (S32A, S36A), Yusuke Nakamura (The University of Tokyo) for *Rrm2b*$^{-/-}$ fibroblasts, and Yafan Wang for searching MM specimens in TLR core. Research was supported by the grants from the Lymphoma SPORE to L.C. and Y.Y., the Tim Nesvig Lymphoma Research Foundation to L.C. and Y.Y. and the National Cancer Institute (5R01CA127541) to Y.Y.

References

Bourdon A, Minai L, Serre V, Jais JP, Sarzi E, Aubert S, Chretien D, de Lonlay P, Paquis-Flucklinger V, Arakawa H, et al. Mutation of RRM2B, encoding p53-controlled ribonucleotide reductase (p53R2), causes severe mitochondrial DNA depletion. Nature genetics. 2007; 39:776–780. [PubMed: 17486094]

Chang L, Zhou B, Hu S, Guo R, Liu X, Jones SN, Yen Y. ATM-mediated serine 72 phosphorylation stabilizes ribonucleotide reductase small subunit p53R2 protein against MDM2 to DNA damage. Proceedings of the National Academy of Sciences of the United States of America. 2008; 105:18519–18524. [PubMed: 19015526]

Grivennikov S, Karin M. Autocrine IL-6 signaling: a key event in tumorigenesis? Cancer Cell. 2008; 13:7–9. [PubMed: 18167335]

Grivennikov SI, Greten FR, Karin M. Immunity, inflammation, and cancer. Cell. 2010; 140:883–899. [PubMed: 20303878]

Kimura T, Takeda S, Sagiya Y, Gotoh M, Nakamura Y, Arakawa H. Impaired function of p53R2 in Rrm2b-null mice causes severe renal failure through attenuation of dNTP pools. Nature genetics. 2003; 34:440–445. [PubMed: 12858174]

Kumar D, Abdulovic AL, Viberg J, Nilsson AK, Kunkel TA, Chabes A. Mechanisms of mutagenesis in vivo due to imbalanced dNTP pools. Nucleic Acids Res. 2011; 39:1360–1371. [PubMed: 20961955]

Liu X, Lai L, Wang X, Xue L, Leora S, Wu J, Hu S, Zhang K, Kuo ML, Zhou L, et al. Ribonucleotide reductase small subunit M2B prognoses better survival in colorectal cancer. Cancer research. 2011; 71:3202–3213. [PubMed: 21415168]

Maeda S, Kamata H, Luo JL, Leffert H, Karin M. IKKbeta couples hepatocyte death to cytokine-driven compensatory proliferation that promotes chemical hepatocarcinogenesis. Cell. 2005; 121:977–990. [PubMed: 15989949]

Naugler WE, Karin M. The wolf in sheep's clothing: the role of interleukin-6 in immunity, inflammation and cancer. Trends Mol Med. 2008; 14:109–119. [PubMed: 18261959]

Nordlund P, Reichard P. Ribonucleotide reductases. Annu Rev Biochem. 2006; 75:681–706. [PubMed: 16756507]

Powell DR, Desai U, Sparks MJ, Hansen G, Gay J, Schrick J, Shi ZZ, Hicks J, Vogel P. Rapid development of glomerular injury and renal failure in mice lacking p53R2. Pediatr Nephrol. 2005; 20:432–440. [PubMed: 15723268]

Rodier F, Coppe JP, Patil CK, Hoeijmakers WA, Munoz DP, Raza SR, Tanaka H, Arakawa H, Yamaguchi T, Shiraishi K, Fukuda S, Matsui K, Takei Y, Nakamura Y. A ribonucleotide reductase gene involved in a p53-dependent cell-cycle checkpoint for DNA damage. Nature. 2000; 404:42–49. [PubMed: 10716435]

Wu ZH, Shi Y, Tibbetts RS, Miyamoto S. Molecular linkage between the kinase ATM and NF-kappaB signaling in response to genotoxic stimuli. Science. 2006; 311:1141–1146. [PubMed: 16497931]

Zhang K, Wu J, Wu X, Wang X, Wang Y, Zhou N, Kuo ML, Liu X, Zhou B, Chang L, et al. p53R2 inhibits the proliferation of human cancer cells in association with cell-cycle arrest. Mol Cancer Ther. 2011; 10:269–278. [PubMed: 21216934]

Zheng L, Dai H, Zhou M, Li M, Singh P, Qiu J, Tsark W, Huang Q, Kernstine K, Zhang X, et al. Fen1 mutations result in autoimmunity, chronic inflammation and cancers. Nat Med. 2007; 13:812–819. [PubMed: 17589521]

Highlight

1. Constitutive NF-KB and STAT3 Mediate Sustained IL-6 Expression in Rrm2b-Deficient Cells
2. Loss of *Rrm2b* Gene Causes Chromosomal Instability
3. Mice Deficient in Rrm2b Exhibit Elevated IL-6 and Hematologic Disorders
4. IL-6 Deficiency Delayed Disease Onset and Mortality of *Rrm2b*$^{-/-}$ mice

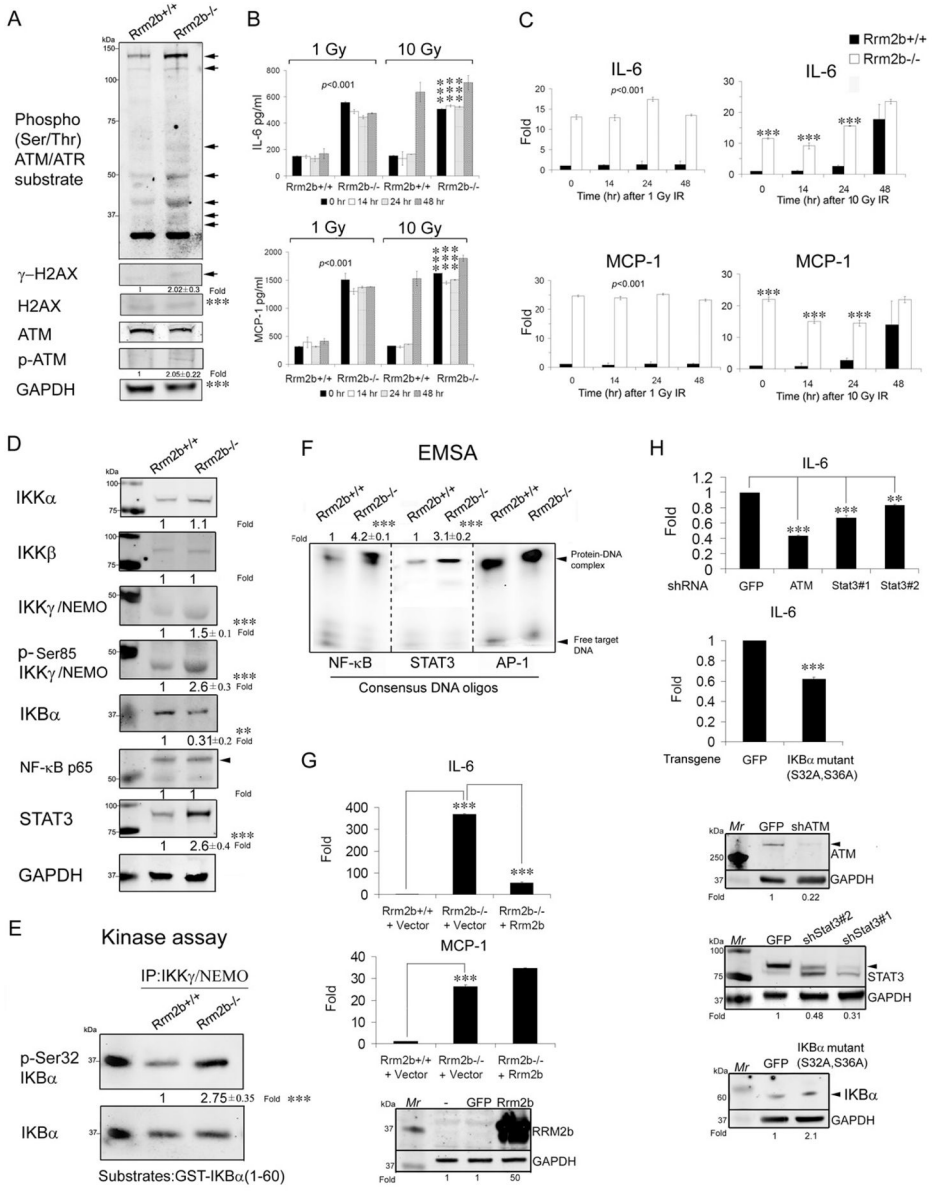

Figure 1. Sustained IL-6 expression mediated by constitutive NF-κB and STAT3 in Rrm2b-deficient Cells

(A) Immunoblotting (IB) analysis of ATM-related signaling proteins in MEFs derived from *Rrm2b*$^{+/+}$ and *Rrm2b*$^{-/-}$ E14.5 embryos. Phosphorylated H2Ax at Ser139, γ-H2AX; Phosphorylated ATM at Ser1981, p-ATM. (B) IL-6 and MCP-1 cytokines from *Rrm2b*$^{+/+}$ and *Rrm2b*$^{-/-}$ MEF media before and after 1 or 10 gray (Gy) IR at the indicated time-points were analyzed by Luminex multiplex cytokine assays. (C) RT-qPCR analysis of *IL-6* and *MCP-1* mRNAs of MEFs before and after 1 or 10 Gy IR. (D) IB analysis of NF-KB and STAT3 signaling proteins in MEFs from each genotype. (E) IKK kinase activity in MEFs of each genotype analyzed by the IKKγ–immunoprecipitated complex on GST-IKBα(1-60) recombinant proteins followed by IB with p-Ser32 IKBα and IKBα antibodies. (F) NF-kB and STAT3 DNA binding activity in MEFs from each genotype analyzed by a non-radioactive electrophoretic mobility shift assay (EMSA) after quantification and normalization with AP-1 binding activity, which served as a control for extract quality and

loading. (G) RT-qPCR analysis of *IL-6* and *MCP-1* mRNAs in *Rrm2b*$^{-/-}$ fibroblasts after infection with lentiviral *Rrm2b* transgenes. Transgene proteins were examined by IB in the bottom panel. (H) RT-qPCR analysis of *IL-6* mRNA in *Rrm2b*$^{-/-}$ MEFs after infection with lentiviruses expressing shRNAs against the indicated target genes or GFP (control). Knocked-down proteins were analyzed by IB and shown in the bottom panels. The fold-chang (Fold) in IB, kinase activity, and EMSA assays is a relative value to WT control after subtraction from the loading control, which given was given an arbitrary value of 1.0. Data represented as mean ± standard deviation (SD) were average from three independent MEFs derived from different embryos for each genotype. **,$p < 0.01$; ***,$p < 0.001$. See also Figure S1.

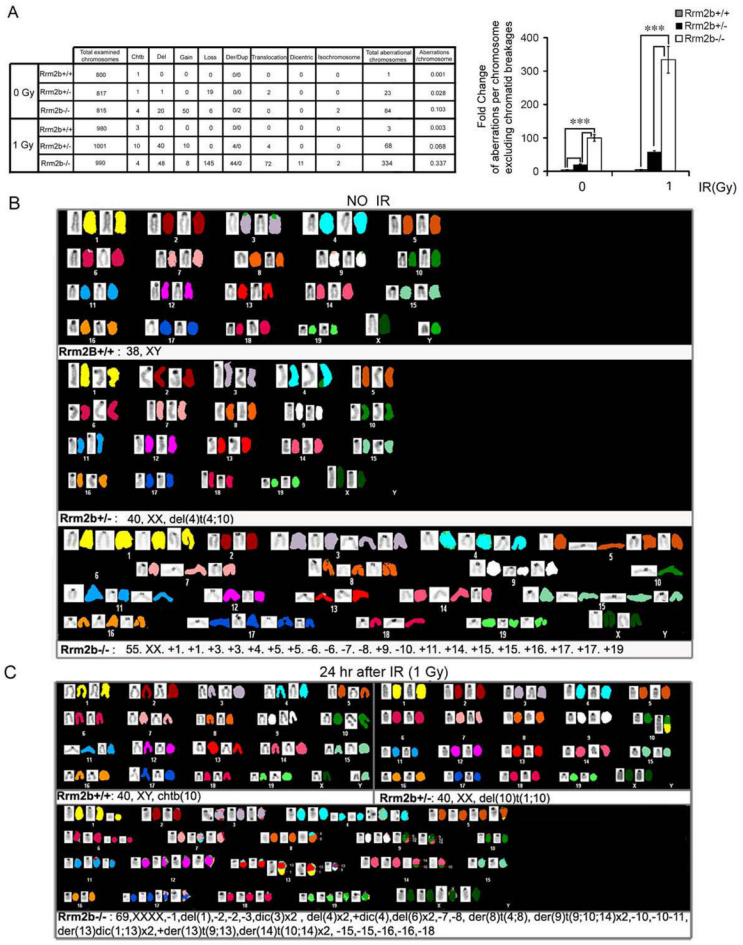

		Total examined chromosomes	Chtb	Del	Gain	Loss	Der/Dup	Translocation	Dicentric	Isochromosome	Total aberrational chromosomes	Aberrations /chromosome
0 Gy	Rrm2b+/+	800	1	0	0	0	0/0	0	0	0	1	0.001
	Rrm2b+/-	817	1	1	0	19	0/0	2	0	0	23	0.028
	Rrm2b-/-	815	4	20	50	6	0/2	0	0	2	84	0.103
1 Gy	Rrm2b+/+	980	3	0	0	0	0/0	0	0	0	3	0.003
	Rrm2b+/-	1001	10	40	10	0	4/0	4	0	0	68	0.068
	Rrm2b-/-	990	4	48	8	145	44/0	72	11	2	334	0.337

Figure 2. Increased Numerical and Structural Chromosome Abnormalities in Rrm2b Deficient Cells

(A) The values in the Table represent the number of each different type of aberrant chromosomes in the examined total chromosomes from three independent cell lines before and 24 h after 1Gy IR for each genotype analyzed by FISH karyotype analysis. The fold-chang of chromosome aberration frequencies excluding Chtb among the genotypes was shown in the histograms. Chromatid break, Chtb; Deletion, del; Extra copies of chromosomes, gain; Missing copies of chromosomes, loss; Derivative chromosome, der; Duplicated chromosome, dup; Chromosomes having two centromeres, dicentric; Fusion of chromosomes, isochromosome. A representative pseudocolor spectral karyotype image of one MEF from each genotype before (B) and 24 h after 1 Gy IR (C). Gain, +; Loss, −; Translocation, t; Dicentric, dic. Data represented as mean ± SD. ***, $p < 0.001$. See also Figure S2.

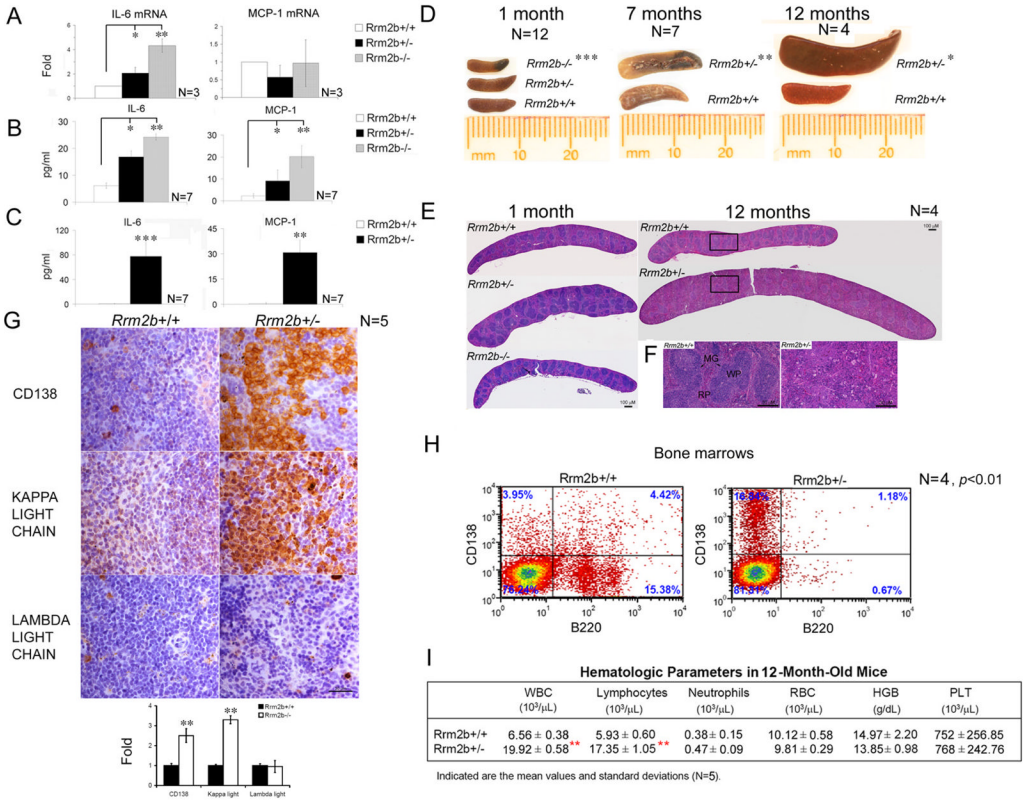

Figure 3. Elevated IL-6 and MCP-1 and the Plasma Cell Neoplasia Phenotype in Aged *Rrm2b*$^{+/-}$ mice

IL-6 and *MCP-1* (A) mRNAs in 1-month-old bone marrows from each genotype analyzed by qPCR. IL-6 and MCP-1 protein levels from blood serum of 1-month-old (B) and from 9- to 12-month-old mice (C). (D) Spleens from each genotype at the indicated ages. The data shown were obtained from a litter-matched group of mice. (E) Tiling images of representative H&E stained sections of spleen from each genotype at 1 and 12 months. Higher magnification of the boxed area of 12-month-old spleens is shown in (F) Marginal Zone, MG; White pulp, WP; Red pulp, RP. (G) A representative section of IHC staining for CD138, KAPPA light chain and LAMBDA light chain antibodies (Brown color) from 12-month-old *Rrm2b*$^{+/+}$ and *Rrm2b*$^{+/-}$ spleens. (H) Fluorescence-activated cell sorting (FACS) of cells derived from *Rrm2b*$^{+/+}$ and *Rrm2b*$^{+/-}$ primary bone marrows for plasma cells using CD138 and B220 antibodies. (I) CBC of peripheral blood from 12-month-old mice. White blood cell, WBC; Red blood cell, RBC; Hemoglobin, HBG; Platelet, PLT. Data represented as mean ± SD. *, $p < 0.05$; **, $p < 0.01$; ***, $p < 0.001$. See also Figure S3.

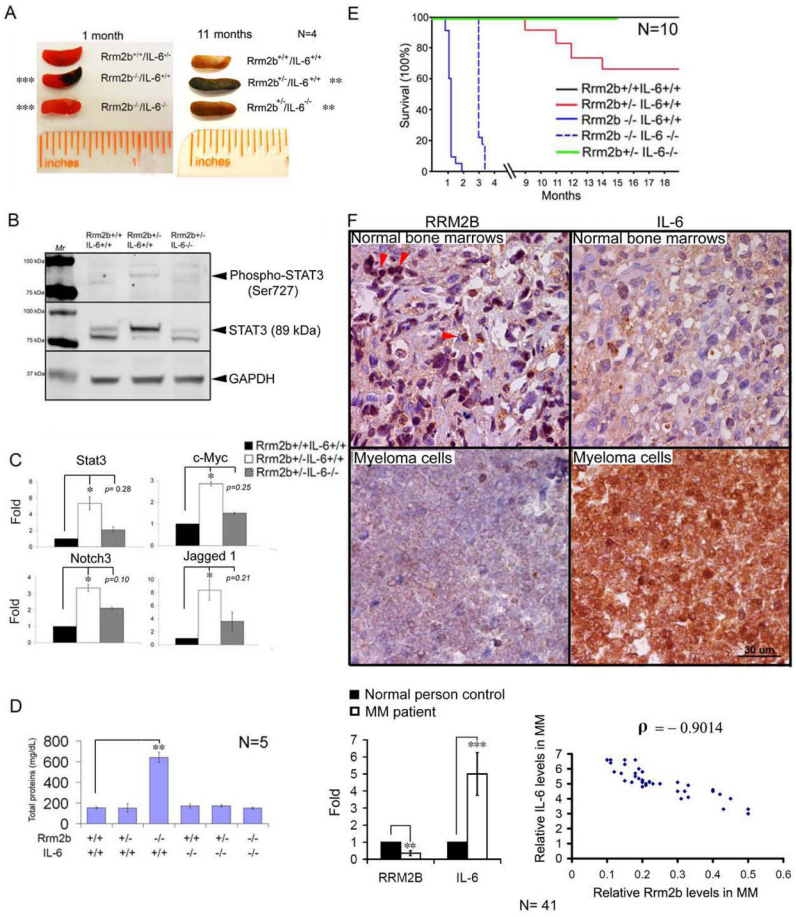

Figure 4. IL-6 Deficiency Delayed Disease Onset and Mortality of *Rrm2b*$^{-/-}$ mice

(A) Absence of splenic hemorrhage in the representative 1-month-old *Rrm2b*$^{-/-}$*IL-6*$^{-/-}$ spleen and 11-month-old *Rrm2b*$^{+/-}$*IL-6*$^{-/-}$ spleen compared to their age-matched littermates. (B) Analysis of STAT3 activity and protein expression in 12-month-oldbone marrows with indicated genotypes by IB analysis using antibodies against phospho-STAT3 (Ser727) and STAT3. (C) mRNA levels of the indicated genes in 12-month-old bone marrows with indicated genotypes. (D) Deletion of *IL-6* blocked urinary protein secretion in *Rrm2b*$^{-/-}$ mice at 5 weeks of age. (E) Kaplan-Meier survival curve of mice with indicated genotypes. (F) A representative section of IHC staining for Rrm2b and IL-6 antibodies (Brown color) from normal human bone marrows and myeloma cells of a MM patient (N=41). Nuclear Rrm2b indicated by arrow heads. The quantification of Rrm2b and IL-6 signals was shown in the histogram. Correlation between relative IL-6 and Rrm2b levels in MM patients was plotted and analyzed by Pearson correlation coefficient analyses. ρ denotes Pearson's correlation. Data represented as mean ± SD. *,p< 0.05; **,p< 0.01; ***,p< 0.001. See also Figure S4.